A steady solution of the gasar eutectic growth in directional solidification*

Li Xiang-Ming(李向明)†, Li Wen-Qiong(李文琼), Jin Qing-Lin(金青林), and Zhou Rong(周 荣)

School of Materials Science and Engineering, Kunming University of Science and Technology, Kunming 650093, *China*

(Received 24 October 2012; revised manuscript received 5 January 2013)

This paper presents the general mathematical model on gasar eutectic growth in directional solidification. Using multiple scale expansion and matching method, we obtain the global steady solution of gasar eutectic growth as the Peclet number $\varepsilon \ll 1$, where ε is defined as the ratio of half an inter-pore spacing and solutal diffusion length. We also give the interfacial shape and predict the porosity of gasar eutectic growth. Results show that porosity is mainly dependent on gas pressure above the metal melt, but independent of pulling velocity. Our predicted results are in agreement with experimental data.

Keywords: porosity, solidification, gasar eutectic growth, asymptotic solution

PACS: 81.30.Fb, 66.30.Je, 44.05.+e, 51.10.+y **DOI:** 10.1088/1674-1056/22/7/078101

1. Introduction

A metal–gas solution may be prepared by melting various metals in an atmosphere containing gas at certain pressure to give a desired gas concentration. Then, porous materials can be produced by solidifying the melts dissolving gas. Gas pores form mainly due to volumetric shrinkage and differences in gas solubility in liquid phase and solid phase. Based on the higher solubility in liquid phase compared with that in solid phase, Shapovalov[1] first produced ordered porous metals named gasars under unidirectional solidification. Later, many researchers[2–4] did similar experiments and prepared gasars with desirable gas morphology. A review the fabrication, properties, and applications of porous metals is given in Ref. [4].

Solidification of metal–gas materials is generally acknowledged to be controlled by a diffusion-limited process and obeys the equilibrium phase diagram shown in Fig. 1. For example, a copper–hydrogen system is similar to eutectic transformations. In order to reveal the essence of gasar formation, diffusion of gas dissolved in metal melt into pores and solidification of metal are considered simultaneously. To understand the formulation of ordered porous metallic materials, some theories are developed to determine porosity and interpore spacing.[3,5–7] Especially, Liu *et al.*[6] presented simple analytical results derived from the eutectic growth theory developed by Jackson and Hunt.[8] However, they only considered the planar liquid–solid and gas–liquid interfaces in their models.

Interfacial morphology formed in the process of solidification has very important effects on the final material structure and properties.[9–13] In the present work, we will present a general mathematical formulation and give the global steady analytical solution using the multiple scale expansion and matching method.[14–17] The present paper is arranged as follows. In Section 2, we give the mathematical formulation of gasar eutectic growth under directional solidification. In Section 3, we present a dimensionless mathematical formulation of steady gasar eutectic growth and derive the solution of the system. We discuss the effects of control conditions on porosity, and further conduct the numerical calculations for a steady solution based on the system of Cu–H_2. In Section 4, we give our conclusions.

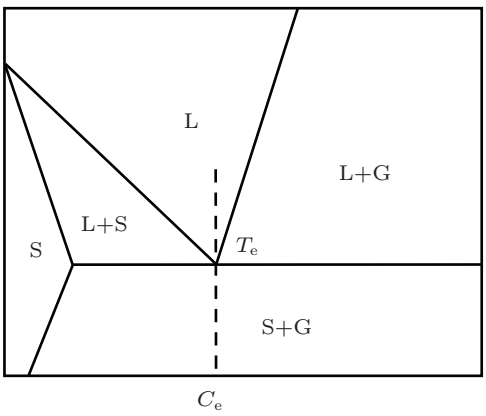


Fig. 1. Schematic phase diagram of a metal–gas system (S: solid, L: liquid, G: gas).

2. Mathematical formulation of gasar eutectic growth

Experimental results show that gas pores form cylinders embedded in the solid metal under directional solidification. Hence, for system of gasar eutectic growth under continuous casting technics, we adopt the cylindrical coordinate system (r, z, θ) moving with pulling speed V in the z direction,

*Project supported by the National Natural Science Foundation of China (Grant Nos. 51201078, 51164018, and u0837603).

†Corresponding author. E-mail: lixiangming04@163.com

© 2013 Chinese Physical Society and IOP Publishing Ltd

as shown in Fig. 2(a). In coordinate system (r,z,θ), the r axis passes through tri-junctions. Considering a system of directional solidification, we can assume that heat conductivity is the same for all phases and the temperature field is only fixed by the experimental setup. The temperature field obeys Laplace's equation

$$\nabla^2 T = 0. \tag{1}$$

In a frame which uniformly translates along the z axis at the pulling velocity V of sample, this quasi-steady state approximation of temperature field is justified on the basis that the thermal diffusion length is large compared to the solutal diffusion length. More detail about the process has been given in Ref. [18]. For directional solidification experiments, a hot zone and a cold zone induce a temperature gradient G to the system directed along the z direction. Hence, the temperature is given by

$$T = T_{\rm e} + G(z - z_*). \tag{2}$$

Here, $T_{\rm e}$ is the gasar eutectic temperature, corresponding to the intersection of liquidus line and solubility line, as shown in Fig. 1, and the undetermined constant z_* is the location of gasar eutectic temperature. Gasar eutectic temperature $T_{\rm e}$ and concentration $C_{\rm e}$ in unit of mole/m^3 are dependent on gas pressure, which are the roots of the following equations:

$$\begin{cases} T = T_{\rm m} + m_{\rm s} C, \\ C = \dfrac{2\rho A_1}{M_{\rm g}} {\rm e}^{(A_2/T)} \sqrt{P_{\rm g}}, \end{cases} \tag{3}$$

where A_1 and A_2 are fixed constants, subscripts s and g represent the solid and gas phase, C is the concentration in liquid phase, $M_{\rm g}$ is the mole mass of gas, ρ is the density of metal melt, $T_{\rm m}$ is the solidification temperature of pure metal, $m_{\rm s}$ is the liquidus slope, and $P_{\rm g}$ is the pressure of gas dissolving in a metal melt. The first expression of Eq. (3) approximately denotes the liquidus line, while the second one is the solubility line.[2]

The temperature of a solid–liquid interface is given by the Gibbs–Thomson condition[14]

$$T = T_{\rm e} + T_{\rm e} \frac{\gamma_{\rm s}}{\Delta H_{\rm s}} \mathscr{K} + m_{\rm s}(C - C_{\rm e}), \tag{4}$$

where

$$\mathscr{K}\{h\} = \frac{\left[r^2 + \left(\dfrac{\partial h}{\partial \theta}\right)^2\right] r \dfrac{\partial^2 h}{\partial r^2} - 2r \dfrac{\partial h}{\partial r} \dfrac{\partial h}{\partial \theta} \dfrac{\partial^2 h}{\partial r \partial \theta} + r\left[1 + \left(\dfrac{\partial h}{\partial r}\right)^2\right]\left(r \dfrac{\partial h}{\partial r} + \dfrac{\partial^2 h}{\partial \theta^2}\right) + 2 \dfrac{\partial h}{\partial r}\left(\dfrac{\partial h}{\partial \theta}\right)^2}{\left[\left(\dfrac{\partial h}{\partial \theta}\right)^2 + \left(r \dfrac{\partial h}{\partial r}\right)^2 + r^2\right]^{3/2}} \tag{5}$$

is twice the mean curvature of the interface, and we designate that $\mathscr{K} < 0$ when interfacial finger points to liquid phase side, $\gamma_{\rm s}$ is the surface tension of solid–liquid interface, and $\Delta H_{\rm s}$ is the latent heat of fusion per unit volume.

Temperature at the gas–liquid interface meets the following condition:

$$T = T_{\rm e} + \frac{\gamma_{\rm g} R_0 T_{\rm e}^2}{P_{\rm a} \Delta H_{\rm g}} \mathscr{K} + m_{\rm g}(C - C_{\rm e}), \tag{6}$$

where the solubility line slope $m_{\rm g}$ taken at the gasar eutectic point can be denoted as follows:

$$m_{\rm g} = -\frac{A_2}{C_{\rm e}[\ln(M_{\rm g} C_{\rm e}) - \ln(2\rho A_1 \sqrt{P_{\rm g}})]^2}. \tag{7}$$

The second term on the right-hand side of Eq. (6) represents the effect of interfacial curvature on the saturation temperature,[5] where $\gamma_{\rm g}$ is the surface tension of gas–liquid interface, $\Delta H_{\rm g}$ is the heat of reaction at which gas dissolves into the liquid metal, and R_0 is the gas constant. The total pressure of gas mixture $P_{\rm a}$ is expressed as

$$P_{\rm a} = P_{\rm g} + P_{\rm o}, \tag{8}$$

where $P_{\rm o}$ is the pressure of other gas that does not dissolve in metal melts.

For the gasar eutectic system, the growth process is controlled by solute transport to be much slower than that of heat. The solute diffusion flux at the interface can be denoted by solute mass balance conditions. At the gas–liquid interface,

$$\begin{aligned} &(C - C_{\rm g})\left(\frac{\partial h_{\rm g}}{\partial t} + V\right) \\ &= -\kappa_{\rm D}\left(\frac{\partial C}{\partial z} - \frac{\partial h_{\rm g}}{\partial r}\frac{\partial C}{\partial r} - \frac{1}{r^2}\frac{\partial h_{\rm g}}{\partial \theta}\frac{\partial C}{\partial \theta}\right), \end{aligned} \tag{9}$$

and at the solid–liquid interface,

$$\begin{aligned} &(1 - \kappa_{\rm s}) C\left(\frac{\partial h_{\rm s}}{\partial t} + V\right) \\ &= -\kappa_{\rm D}\left(\frac{\partial C}{\partial z} - \frac{\partial h_{\rm s}}{\partial r}\frac{\partial C}{\partial r} - \frac{1}{r^2}\frac{\partial h_{\rm s}}{\partial \theta}\frac{\partial C}{\partial \theta}\right), \end{aligned} \tag{10}$$

where $C_{\rm g}$ is the concentration in gas pore, $\kappa_{\rm D}$ is the solute diffusivity, and $\kappa_{\rm s}$ is the partition coefficient.

It is noted that we neglect the diffusion in the gas phase in Eq. (9). Using the ideal gas law, we can approximatively

denote the concentration in a gas pore as

$$C_{\rm g} = w\frac{2P_{\rm a}}{R_0 T_{\rm e}}. \tag{11}$$

Here, we neglect hydrostatic pressure and an extra pressure caused by the curvature of the gas–melt interface, which are very smaller than the external pressure $P_{\rm a}$. The w is the modified factor, and we will discuss it in next section. For simplicity, we also neglect the diffusion in the solid phase in Eq. (10) because its diffusion coefficient is much smaller than one in liquid phase.

The concentration field in the liquid phase meets

$$\kappa_{\rm D}\nabla^2 C + V\frac{\partial C}{\partial z} = \frac{\partial C}{\partial t}. \tag{12}$$

At the tri-junctions, local equilibrium requires that the surface tensions balance as expressed by Young's law

$$\begin{cases} \gamma_{\rm g}\sin\theta_{\rm g} + \gamma_{\rm s}\sin\theta_{\rm s} = \gamma_{\rm gs}, \\ \gamma_{\rm g}\cos\theta_{\rm g} - \gamma_{\rm s}\cos\theta_{\rm s} = 0, \end{cases} \tag{13}$$

where $\gamma_{\rm gs}$ is the surface tension of solid–gas interface. The contact angles $\theta_{\rm g}$ and $\theta_{\rm s}$ are determined by this condition.

Another important condition is that the initial concentration of melt C_∞ meets[2]

$$C_\infty = \frac{2\rho A_1}{M_{\rm g}} {\rm e}^{(A_2/T_{\rm h})}\sqrt{P_{\rm g}}, \tag{14}$$

where $T_{\rm h}$ is the temperature of the hot zone.

3. Steady solution of gasar eutectic growth

In the previous section, we have given the general mathematical formulation of gasar eutectic growth. We will obtain the steady solution of the above mathematical model in this section. One can use half of inter-pore spacing, R, as the length scale and pulling velocity V as the velocity scale. The scales of temperature T and concentration C are set as $\Delta H_{\rm s}/(c_{\rm p}\rho)$ and $C_{\rm e}$, respectively. The $c_{\rm p}$ is the specific heat. We define the non-dimensional temperature field as $\bar{T} = (T - T_{\rm e})((c_{\rm p}\rho)/\Delta H_{\rm s})$, and the dimensionless concentration field as $\bar{C} = (C - C_{\rm e})/C_{\rm e}$. Substituting these dimensionless parameters into the above system, one can easily obtain the dimensionless form. Due to the steady solution of gasar eutectic growth given in this paper, we only present the dimensionless mathematical formulation of steady gasar eutectic growth. Obviously, as gasar eutectic grows steadily, the pulling velocity will be equal to the growth velocity of the interface.

For a system of axi-symmetric gasar eutectic growth, due to periodicity of the solution, we may only consider a cell in cylindrical coordinate system $(\bar{r}, \bar{z})$ as shown in Fig. 2(a). Following the theory of eutectic growth given by Jackson and Hunt,[8] we replace a hexagon boundary by a circle of equivalent area shown in Fig. 2(b). In this case, the problem is equivalent to gasar eutectic growth in a channel with fixed cylinder $\bar{r} = 1$.

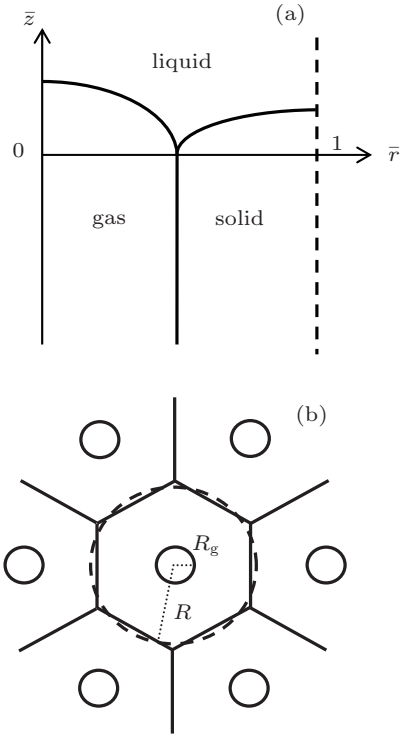


Fig. 2. Geometry model of gasar eutectic growth. (a) Axi-symmetric gasar eutectic growth with fixed cylinder $\bar{r} = 1$ in cylindrical coordinate system $(\bar{r}, \bar{z}, \theta)$; (b) transversal surface of gasar eutectic structure.

The dimensionless concentration field $\bar{C}(\bar{r}, \bar{z})$ is subjected to the following system in cylindrical coordinate system $(\bar{r}, \bar{z})$:

$$\frac{\partial^2 \bar{C}}{\partial \bar{r}^2} + \frac{1}{\bar{r}}\frac{\partial \bar{C}}{\partial \bar{r}} + \frac{\partial^2 \bar{C}}{\partial \bar{z}^2} + \varepsilon\frac{\partial \bar{C}}{\partial \bar{z}} = 0, \tag{15}$$

where the Peclet number ε is defined as

$$\varepsilon = \frac{RV}{\kappa_{\rm D}}. \tag{16}$$

The boundary conditions are given as follows:

i) as $\bar{z} \to \infty$,

$$\bar{C} \to \bar{C}_\infty; \tag{17}$$

ii) as $\bar{r} = 0, 1$,

$$\frac{\partial \bar{C}}{\partial \bar{r}} = \frac{\partial \bar{h}}{\partial \bar{r}} = 0; \tag{18}$$

iii) at the interface, $\bar{z} = \bar{h}(\bar{r})$, the Gibbs–Thomson condition is given by

$$\bar{C} = -\varepsilon\frac{\bar{G}}{\mathbb{M}}(\bar{h} - \bar{z}_*) + \frac{\Gamma}{\varepsilon\mathbb{M}}\bar{\mathscr{K}}\{\bar{h}\}, \tag{19}$$

and the solute mass balance condition is given by

$$\frac{\partial \bar{C}}{\partial \bar{z}} - \frac{\partial \bar{h}_{\rm s}}{\partial \bar{r}}\frac{\partial \bar{C}}{\partial \bar{r}} + \varepsilon(1 - \kappa_{\rm s})(\bar{C} + 1) = 0, \tag{20}$$

$$\frac{\partial \bar{C}}{\partial \bar{z}} - \frac{\partial \bar{h}_{\rm g}}{\partial \bar{r}}\frac{\partial \bar{C}}{\partial \bar{r}} + \varepsilon(\bar{C} - \bar{C}_{\rm g}) = 0, \tag{21}$$

where

$$\Gamma = \begin{cases} \Gamma_{\rm g} = \dfrac{\gamma_{\rm g} R_0 c_{\rm p} \rho T_{\rm e}^2 V}{P_{\rm l} \Delta H_{\rm g} \Delta H_{\rm s} \kappa_{\rm D}}, & 0 < \bar{r} < \bar{r}_*, \\ \Gamma_{\rm s} = \dfrac{\gamma_{\rm s} c_{\rm p} \rho T_{\rm e} V}{(\Delta H_{\rm s})^2 \kappa_{\rm D}}, & \bar{r}_* < \bar{r} < 1, \end{cases} \tag{22}$$

$$\mathbb{M} = \begin{cases} \mathbb{M}_{\rm g} = -\dfrac{m_{\rm g} C_{\rm e}}{\Delta H_{\rm s}/(c_{\rm p}\rho)}, & 0 < \bar{r} < \bar{r}_*, \\ \mathbb{M}_{\rm s} = -\dfrac{m_{\rm s} C_{\rm e}}{\Delta H_{\rm s}/(c_{\rm p}\rho)}, & \bar{r}_* < \bar{r} < 1, \end{cases} \tag{23}$$

$$\bar{r}_* = \frac{R_{\rm g}}{R}, \quad \bar{G} = \frac{\kappa_{\rm D} G}{V \Delta H_{\rm s}/(c_{\rm p}\rho)}, \tag{24}$$

and $R_{\rm g}$ is the radius of gas pore;

iv) at the tri-junctions, $\bar{r} = \bar{r}_*$, $\bar{h}(\bar{r}_*) = 0$, and

$$\begin{cases} \dfrac{\partial \bar{h}_{\rm g}}{\partial \bar{r}} = -\tan\theta_{\rm g}, \\ \dfrac{\partial \bar{h}_{\rm s}}{\partial \bar{r}} = \tan\theta_{\rm s}. \end{cases} \tag{25}$$

3.1. Steady state solution in region far from interface

We will obtain the steady asymptotic solution of the above system using multiple scale expansion and matching method. Mostly, eutectic spacing is very small compared with the length of the solute diffusion, so we can let the small parameter $\varepsilon \ll 1$. That is to say, the boundary of solute diffusion is much larger than R. As $\bar{z} \gg O(1)$, the diffusion in the region far from the solute diffusion boundary is not effected by the interface shape, so the concentration field is independent of the variable $\bar{r}$, and the interface may be considered as planar. We will divide the liquid region into two sub-regions: outer region far from interface; inner region. One can obtain solutions in different sub-regions, then match these two solutions, and finally derive the global solution in the whole system. In this subsection, we first attempt to find the solution in the outer region.

We introduce the outer variable as

$$\hat{z} = \varepsilon \bar{z}, \tag{26}$$

then Eq. (15) is changed into

$$\frac{\partial^2 \bar{C}_{\rm O}}{\partial \hat{z}^2} + \frac{\partial \bar{C}_{\rm O}}{\partial \hat{z}} = 0, \tag{27}$$

with the following boundary conditions:

$$\bar{C}_{\rm O} \to \bar{C}_\infty, \quad \bar{z}, \hat{z} \to \infty. \tag{28}$$

We expand the outer solution in the following asymptotic form, as $\varepsilon \to 0$:

$$\bar{C}(\bar{r}, \hat{z}) = \bar{C}_{\rm O}(\hat{z}) = \bar{C}_{\rm O1}(\hat{z}) + \varepsilon \bar{C}_{\rm O2}(\hat{z}) + \cdots. \tag{29}$$

The solution of the above system can be easily derived as

$$\bar{C}_{\rm O} = \bar{C}_\infty [1 - D_0 \exp(-\hat{z})] + \varepsilon D_1 \exp(-\hat{z}) + \cdots, \tag{30}$$

where D_0 and D_1 are undetermined constants.

3.2. Solution in inner region

In the inner region, the system is given by

$$\frac{\partial^2 \bar{C}}{\partial \bar{r}^2} + \frac{1}{\bar{r}} \frac{\partial \bar{C}}{\partial \bar{r}} + \frac{\partial^2 \bar{C}}{\partial \bar{z}^2} + \varepsilon \frac{\partial \bar{C}}{\partial \bar{z}} = 0, \tag{31}$$

with the following boundary conditions.

i) As $\bar{z} \to \infty$,

$$\bar{C} \to 0. \tag{32}$$

ii) As $\bar{r} = 0, 1$,

$$\frac{\partial \bar{C}}{\partial \bar{r}} = \frac{\partial \bar{h}}{\partial \bar{r}} = 0. \tag{33}$$

iii) At the interface, $\bar{z} = \bar{h}(\bar{r})$, and the Gibbs–Thomson condition is given by

$$\bar{C} = -\varepsilon \frac{\bar{G}}{\mathbb{M}} (\bar{h} - \bar{z}_*) + \frac{\Gamma}{\varepsilon \mathbb{M}} \mathscr{K} \{\bar{h}\}, \tag{34}$$

and the solute mass balance condition is given by

$$\frac{\partial \bar{C}}{\partial \bar{z}} - \frac{\partial \bar{h}_{\rm s}}{\partial \bar{r}} \frac{\partial \bar{C}}{\partial \bar{r}} + \varepsilon (1 - \kappa_{\rm s})(\bar{C} + 1) = 0, \tag{35}$$

$$\frac{\partial \bar{C}}{\partial \bar{z}} - \frac{\partial \bar{h}_{\rm g}}{\partial \bar{r}} \frac{\partial \bar{C}}{\partial \bar{r}} + \varepsilon (\bar{C} - \bar{C}_{\rm g}) = 0. \tag{36}$$

iv) At the tri-junctions, $\bar{r} = \bar{r}_*$, $\bar{h}(\bar{r}_*) = 0$, and

$$\begin{cases} \dfrac{\partial \bar{h}_{\rm g}}{\partial \bar{r}} = -\tan\theta_{\rm g}, \\ \dfrac{\partial \bar{h}_{\rm s}}{\partial \bar{r}} = \tan\theta_{\rm s}. \end{cases} \tag{37}$$

It is very difficult to obtain the exact solution of above system. Here we will obtain the asymptotic solution. Generally, $\mathbb{M}$ and Γ are small parameters. For example, for system of Cu–H_2, $0.001 \le \mathbb{M} \le 0.1$, and $10^{-7} \le \Gamma \le 10^{-4}$. As usual, we write Γ as follows:[15]

$$\Gamma = \varepsilon^2 \hat{\Gamma}, \tag{38}$$

where $\hat{\Gamma} = O(1)$. We also assume that the amplitude of the interface $|\bar{h}|$ is small, and

$$|\bar{h}| = O(\mathbb{M}_{\rm s}).$$

We expand the concentration field $\bar{C}(\bar{r}, \bar{z})$, interface function $\bar{h}(\bar{r})$, and $\bar{z}_*$ in the following form:

$$\begin{cases} \bar{C}(\bar{r}, \bar{z}) = \bar{C}_{\rm I}(\bar{r}, \bar{z}) = \mu_1(\varepsilon) \bar{C}_{\rm I1}(\bar{r}, \bar{z}) + \mu_2(\varepsilon) \bar{C}_{\rm I2}(\bar{r}, \bar{z}) + \cdots, \\ \bar{h}(\bar{r}) = \delta_1(\varepsilon) \bar{h}_{\rm I1}(\bar{r}) + \delta_2(\varepsilon) \bar{h}_{\rm I2}(\bar{r}) + \cdots, \\ \bar{z}_* = \nu_1(\varepsilon) \bar{z}_{*1} + \nu_2(\varepsilon) \bar{z}_{*2} + \cdots, \end{cases} \tag{39}$$

and as $\varepsilon \to 0$,

$$1 \gg \mu_1(\varepsilon) \gg \mu_2(\varepsilon) \gg \cdots,$$
$$1 \gg \delta_1(\varepsilon) \gg \delta_2(\varepsilon) \gg \cdots,$$
$$1 \gg \nu_1(\varepsilon) \gg \nu_2(\varepsilon) \gg \cdots.$$

By substituting Eq. (39) into systems (31)–(37), we can derive approximate solutions of each order. Next, we will give the first-order approximation.

The first approximation of the solute diffusion equation is

$$\frac{\partial^2 \bar{C}_{\mathrm{I}1}}{\partial \bar{r}^2}+\frac{1}{\bar{r}}\frac{\partial \bar{C}_{\mathrm{I}1}}{\partial \bar{r}}+\frac{\partial^2 \bar{C}_{\mathrm{I}1}}{\partial \bar{z}^2}=0, \tag{40}$$

with the following boundary conditions.

i) At $\bar{r}=0,1$,

$$\frac{\partial \bar{C}_{\mathrm{I}1}}{\partial \bar{r}}=\frac{\partial \bar{h}_{\mathrm{I}1}}{\partial \bar{r}}=0. \tag{41}$$

From Eqs. (35) and (36), we can derive that $\mu_1(\varepsilon)=\varepsilon$, and $\delta_1(\varepsilon)=\nu_1(\varepsilon)=\mathbb{M}_{\mathrm{s}}$.

ii) At the interface, we have $\bar{z}=\bar{h}(\bar{r})=O(\delta_1)$. Therefore, the interface conditions can be linearized at $\bar{z}=0$. The Gibbs–Thomson condition is given by

$$\bar{C}_{\mathrm{I}1}=-\frac{\bar{G}}{\hat{\mathbb{M}}}(\bar{h}_{\mathrm{I}1}-\bar{z}_{*1})+\frac{\hat{\Gamma}}{\hat{\mathbb{M}}}\Big(\frac{\partial^2 \bar{h}_{\mathrm{I}1}}{\partial \bar{r}^2}+\frac{1}{\bar{r}}\frac{\partial \bar{h}_{\mathrm{I}1}}{\partial \bar{r}}\Big), \tag{42}$$

where

$$\hat{\mathbb{M}}=\begin{cases}\dfrac{\mathbb{M}_{\mathrm{g}}}{\mathbb{M}_{\mathrm{s}}}, & 0<\bar{r}<\bar{r}_*,\\ 1, & \bar{r}_*<\bar{r}<1,\end{cases} \tag{43}$$

and the solute mass balance condition is given by

$$\frac{\partial \bar{C}_{\mathrm{I}1}}{\partial \bar{z}}+(1-\kappa_{\mathrm{s}})=0, \tag{44}$$

$$\frac{\partial \bar{C}_{\mathrm{I}1}}{\partial \bar{z}}-\bar{C}_{\mathrm{g}}=0. \tag{45}$$

iii) As $\bar{r}=\bar{r}_*$,

$$\begin{cases}\bar{h}'_{\mathrm{I}1\mathrm{g}}(\bar{r}_*)=\Theta_{\mathrm{g}},\\ \bar{h}'_{\mathrm{I}1\mathrm{s}}(\bar{r}_*)=\Theta_{\mathrm{s}},\\ \bar{h}_{\mathrm{I}1\mathrm{g}}(\bar{r}_*)=\bar{h}_{\mathrm{I}1\mathrm{s}}(\bar{r}_*)=0,\end{cases} \tag{46}$$

where $\tan\theta_{\mathrm{g}}=-\mathbb{M}_{\mathrm{s}}\Theta_{\mathrm{g}}$, and $\tan\theta_{\mathrm{s}}=\mathbb{M}_{\mathrm{s}}\Theta_{\mathrm{s}}$. The general solution of Eq. (40) is

$$\bar{C}_{\mathrm{I}1}=D_2+D_3\bar{z}+\sum_{n=1}^{\infty}\hat{C}_n\mathrm{J}_0(\lambda_n\bar{r})\exp(-\lambda_n\bar{z}), \tag{47}$$

where $\mathrm{J}_n(x)$ is the Bessel function of the first kind, λ_n is the positive root of $\mathrm{J}_1(x)$, D_2 and D_3 are undetermined constants.

Substituting Eq. (47) into Eqs. (44) and (45) by integrating the above equations and using the orthogonality of $\mathrm{J}_0(x)$, we obtain the Fourier coefficients $\hat{C}_n$ as

$$\hat{C}_n=-\frac{2(1-\kappa_{\mathrm{s}}+\bar{C}_{\mathrm{g}})\bar{r}_*\mathrm{J}_1(\bar{r}_*\lambda_n)}{\lambda_n^2\mathrm{J}_0^2(\lambda_n)}, \tag{48}$$

$$\bar{r}_*=\sqrt{\frac{1-\kappa_{\mathrm{s}}+D_3}{1-\kappa_{\mathrm{s}}+\bar{C}_{\mathrm{g}}}}. \tag{49}$$

Next, we determine the interfacial function $\bar{h}_{\mathrm{I}1}$. From the Gibbs–Thomson condition (34), we have

$$\frac{\hat{\Gamma}}{\hat{\mathbb{M}}}\Big(\frac{\partial^2 \bar{h}_{\mathrm{I}1}}{\partial \bar{r}^2}+\frac{1}{\bar{r}}\frac{\partial \bar{h}_{\mathrm{I}1}}{\partial \bar{r}}\Big)-\frac{\bar{G}}{\hat{\mathbb{M}}}(\bar{h}_{\mathrm{I}1}-\bar{z}_{*1})=D_2+\sum_{n=1}^{\infty}\hat{C}_n\mathrm{J}_0(\lambda_n\bar{r}),$$

or

$$\bar{r}^2\frac{\partial^2 \bar{h}_{\mathrm{I}1}}{\partial \bar{r}^2}+\bar{r}\frac{\partial \bar{h}_{\mathrm{I}1}}{\partial \bar{r}}-(A\bar{r})^2\bar{h}_{\mathrm{I}1}=f(\bar{r}), \tag{50}$$

where $A^2=\bar{G}/\hat{\Gamma}$ and

$$f(\bar{r})=\frac{\hat{\mathbb{M}}}{\hat{\Gamma}}\bar{r}^2\Big[D_2-\frac{\bar{G}}{\hat{\mathbb{M}}}\bar{z}_{*1}+\sum_{n=1}^{\infty}\hat{C}_n\mathrm{J}_0(\lambda_n\bar{r})\Big]. \tag{51}$$

The general solution of Eq. (50) is

$$\bar{h}_{\mathrm{I}1}(\bar{r})=d_0\mathrm{I}_0(A\bar{r})+d_1\mathrm{K}_0(A\bar{r})+g(\bar{r}), \tag{52}$$

where $\mathrm{I}_n(x)$ and $\mathrm{K}_n(x)$ are the modified Bessel functions of the first and second kind, and

$$\begin{aligned}g_{\mathrm{g}}(\bar{r}) &= A_{\mathrm{g}}\mathrm{I}_0(A_{\mathrm{g}}\bar{r})\int_0^{\bar{r}}\frac{\mathrm{K}_0(A_{\mathrm{g}}r)f_{\mathrm{g}}(r)}{(A_{\mathrm{g}}r)^2[\mathrm{K}_0(A_{\mathrm{g}}r)\mathrm{I}_1(A_{\mathrm{g}}r)+\mathrm{I}_0(A_{\mathrm{g}}r)\mathrm{K}_1(A_{\mathrm{g}}r)]}\,\mathrm{d}r\\ &\quad -A_{\mathrm{g}}\mathrm{K}_0(A_{\mathrm{g}}\bar{r})\int_0^{\bar{r}}\frac{\mathrm{I}_0(A_{\mathrm{g}}r)f_{\mathrm{g}}(r)}{(A_{\mathrm{g}}r)^2[\mathrm{K}_0(A_{\mathrm{g}}r)\mathrm{I}_1(A_{\mathrm{g}}r)+\mathrm{I}_0(A_{\mathrm{g}}r)\mathrm{K}_1(A_{\mathrm{g}}r)]}\,\mathrm{d}r,\end{aligned} \tag{53}$$

$$\begin{aligned}g_{\mathrm{s}}(\bar{r}) &= A_{\mathrm{s}}\mathrm{I}_0(A_{\mathrm{s}}\bar{r})\int_1^{\bar{r}}\frac{\mathrm{K}_0(A_{\mathrm{s}}r)f_{\mathrm{s}}(r)}{(A_{\mathrm{s}}r)^2[\mathrm{K}_0(A_{\mathrm{s}}r)\mathrm{I}_1(A_{\mathrm{s}}r)+\mathrm{I}_0(A_{\mathrm{s}}r)\mathrm{K}_1(A_{\mathrm{s}}r)]}\,\mathrm{d}r\\ &\quad -A_{\mathrm{s}}\mathrm{K}_0(A_{\mathrm{s}}\bar{r})\int_1^{\bar{r}}\frac{\mathrm{I}_0(A_{\mathrm{s}}r)f_{\mathrm{s}}(r)}{(A_{\mathrm{s}}r)^2[\mathrm{K}_0(A_{\mathrm{s}}r)\mathrm{I}_1(A_{\mathrm{s}}r)+\mathrm{I}_0(A_{\mathrm{s}}r)\mathrm{K}_1(A_{\mathrm{s}}r)]}\,\mathrm{d}r.\end{aligned} \tag{54}$$

From Eq. (41), we can determine that

$$d_{\mathrm{g}1}=0,\quad d_{\mathrm{s}0}=d_{\mathrm{s}1}\frac{\mathrm{K}_1(A_{\mathrm{s}})}{\mathrm{I}_1(A_{\mathrm{s}})}, \tag{55}$$

and from Eq. (46), we also obtain

$$d_{\mathrm{g}0}=\frac{\Theta_{\mathrm{g}}-g'_{\mathrm{g}}(\bar{r}_*)}{A_{\mathrm{g}}\mathrm{I}_1(A_{\mathrm{g}}\bar{r}_*)},\quad d_{\mathrm{s}1}=\frac{\mathrm{I}_1(A_{\mathrm{s}})[\Theta_{\mathrm{s}}-g'_{\mathrm{s}}(\bar{r}_*)]}{A_{\mathrm{s}}\mathrm{K}_1(A_{\mathrm{s}})\mathrm{I}_1(A_{\mathrm{s}}\bar{r}_*)-A_{\mathrm{s}}\mathrm{I}_1(A_{\mathrm{s}})\mathrm{K}_1(A_{\mathrm{s}}\bar{r}_*)},$$

$$\bar{z}_{*1} = \frac{\hat{\mathbb{M}}_g \hat{\mathbb{M}}_s (D_{2g} - D_{2s})}{\bar{G}(\hat{\mathbb{M}}_g - \hat{\mathbb{M}}_s)}, \quad D_2 = \frac{\hat{\mathbb{M}}_g D_{2g} - \hat{\mathbb{M}}_s D_{2s}}{\hat{\mathbb{M}}_g - \hat{\mathbb{M}}_s}, \tag{56}$$

where

$$D_{2g} = \Theta_g \frac{\hat{\Gamma}_g}{\hat{\mathbb{M}}_g} \frac{I_0(A_g \bar{r}_*)}{Q_{g2}[I_0(A_g \bar{r}_*)K_1(A_g \bar{r}_*) + K_0(A_g \bar{r}_*)I_1(A_g \bar{r}_*)]} - \frac{P_{g2}}{Q_{g2}},$$

$$D_{2s} = \Theta_s \frac{\hat{\Gamma}_s}{\hat{\mathbb{M}}_s} \frac{K_1(A_s)I_0(A_s \bar{r}_*) + I_1(A_s)K_0(A_s \bar{r}_*)}{[Q_{s1}I_1(A_s) + Q_{s2}K_1(A_s)][K_1(A_s \bar{r}_*)I_0(A_s \bar{r}_*) + I_1(A_s \bar{r}_*)K_0(A_s \bar{r}_*)]} - \frac{P_{s1}I_1(A_s) + P_{s2}K_1(A_s)}{Q_{s1}I_1(A_s) + Q_{s2}K_1(A_s)},$$

$$P_{g2} = \int_0^{\bar{r}_*} \frac{I_0(A_g r) \sum_{n=1}^{\infty} \hat{C}_n J_0(\mu_n r)}{K_0(A_g r)I_1(A_g r) + I_0(A_g r)K_1(A_g r)} \mathrm{d}r,$$

$$Q_{g2} = \int_0^{\bar{r}_*} \frac{I_0(A_g r)}{K_0(A_g r)I_1(A_g r) + I_0(A_g r)K_1(A_g r)} \mathrm{d}r,$$

$$P_{s1} = \int_1^{\bar{r}_*} \frac{K_0(A_s r) \sum_{n=1}^{\infty} \hat{C}_n J_0(\mu_n r)}{K_0(A_s r)I_1(A_s r) + I_0(A_s r)K_1(A_s r)} \mathrm{d}r,$$

$$Q_{s1} = \int_1^{\bar{r}_*} \frac{K_0(A_s r)}{K_0(A_s r)I_1(A_s r) + I_0(A_s r)K_1(A_s r)} \mathrm{d}r,$$

$$P_{s2} = \int_1^{\bar{r}_*} \frac{I_0(A_s r) \sum_{n=1}^{\infty} \hat{C}_n J_0(\mu_n r)}{K_0(A_s r)I_1(A_s r) + I_0(A_s r)K_1(A_s r)} \mathrm{d}r,$$

$$Q_{s2} = \int_1^{\bar{r}_*} \frac{I_0(A_s r)}{K_0(A_s r)I_1(A_s r) + I_0(A_s r)K_1(A_s r)} \mathrm{d}r.$$

So far, only constants D_0, D_1, and D_3 are not determined. We can fix them by matching the outer solution (30) with the inner solution (39). The matching condition is that as $\hat{z} \to 0$ and $\bar{z} \to \infty$,

$$\bar{C}_O(\hat{z}) \Longleftrightarrow \bar{C}_I(\bar{r}, \bar{z}). \tag{57}$$

As $\hat{z} \to 0$,

$$\begin{aligned} \bar{C}_O(\hat{z}) &= \bar{C}_\infty[1 - D_0 \exp(-\hat{z})] + \varepsilon D_1 \exp(-\hat{z}) + O(\text{h.o.t}) \\ &= \bar{C}_\infty[1 - D_0 \exp(-\varepsilon \bar{z})] + \varepsilon D_1 \exp(-\varepsilon \bar{z}) + O(\text{h.o.t}) \\ &= \bar{C}_\infty[1 - D_0] + \varepsilon D_0 \bar{C}_\infty \bar{z} + \varepsilon D_1 + O(\text{h.o.t}), \end{aligned} \tag{58}$$

and as $\bar{z} \to \infty$,

$$\bar{C}_I(\bar{r}, \bar{z}) = \varepsilon[D_2 + D_3 \bar{z} + \sum_{n=1}^{\infty} \hat{C}_n J_0(\lambda_n \bar{r}) \exp(-\lambda_n \bar{z})] + O(\text{h.o.t}). \tag{59}$$

Thus, $D_0 = 1$, $D_3 = \bar{C}_\infty$, and $D_1 = D_2$.

3.3. Results and analysis

We now analyze the steady solution of gasar eutectic growth that we have obtained. We first focus on the effect of gas pressure and temperature of hot zone on porosity. Equation (49) determines the dimensionless radius of gas pore. This equation is derived based on the solutal mass conservation condition. Porosity of gas is equal to $\bar{r}_*^2$. Equation (49) shows that porosity is independent of the pulling speed, which is in agreement with the experimental results,[3] and is determined by C_∞ and C_g. For fixed gasar eutectic temperature, we cannot ensure that the concentration in the gas pore derived by using ideal gas law is the one in actual experiment of unidirectional solidification due to the none-fixed temperature. Hence, we introduce a modified factor w in definition of equivalent concentration in gas pore. We can fix the value of w by using experimental data given in Ref. [3]. The parameters used in our theoretical calculation are shown in Table 1. For $P_g = 1$ MPa, we calculate the average value for all of the experimental data given in Ref. [3], then substitute it into Eq. (49), and obtain $w = 2.1$. For this fixed constant given by using experimental data, we then present relationship of $\bar{r}_*^2$ with control conditions.

Table 1. The thermodynamic characteristics of Cu–H_2.

A_1	0.722×10^{-6} [2]
A_2	-5324.0 [2]
κ_s	0.31 [3]
T_h/K	1573.0 [3]
T_m/K	1357.0
κ_D/m^2·s^{-1}	1.0×10^{-7} [3]
m_s/K·m^3·mol^{-1}	-0.01026 [6]
θ_g	61°
θ_s	35°
γ_g/J·m^{-2}	0.3
γ_s/J·m^{-2}	0.178 [6]
M_g/kg·mol^{-1}	2.016×10^{-3}
R_0/J·mol^{-1}·K^{-1}	8.3145
ρ/kg·m^{-3}	8.0×10^3 [6]
ΔH_g/J·mol^{-1}	7.78×10^4 [5]
ΔH_s/J·m^{-3}	1.695×10^9 [6]
c_p/J·kg^{-1}·K^{-1}	470 [8]

Porosity is mainly dependent on the external pressure and the temperature of the hot zone shown in Fig. 3. Figure 3(a) presents relationship of $\bar{r}_*^2$ with P_g for the case of $T_h = 1573$ K and $P_o = 0$, 0.5, 1, and 2 MPa, respectively. In this figure, we also present the average value of the experimental data for the case of $P_g = 2$ MPa. It is seen that the experimental point

is on our theoretical curve. It is obvious that the porosity decreases with increasing P_g without other gas pressure, and has a maximum for different values of P_o. Figure 3(b) presents relationship of $\bar{r}_*^2$ with P_o for the case of $P_g = 1, 2, 3$ MPa. It is seen that the increase of other gas pressure that not dissolving metal melt leads to decreasing of porosity. In Fig. 3(c), we show the relationship of porosity with T_h. It is seen that porosity increases with increasing T_h.

In Fig. 4, we give shapes of vertical section through symmetry axis $\bar{r} = 0$ for fixed control conditions. It is seen that solid–liquid interface first changes from convex to concave with the increase in the part pressure P_g, and then gas–liquid interface follows. In Fig. 5, we give the relationship of the interfacial tip point location with P_g. It is seen that $h(0)$ and $h(1)$ decrease as P_g increases.

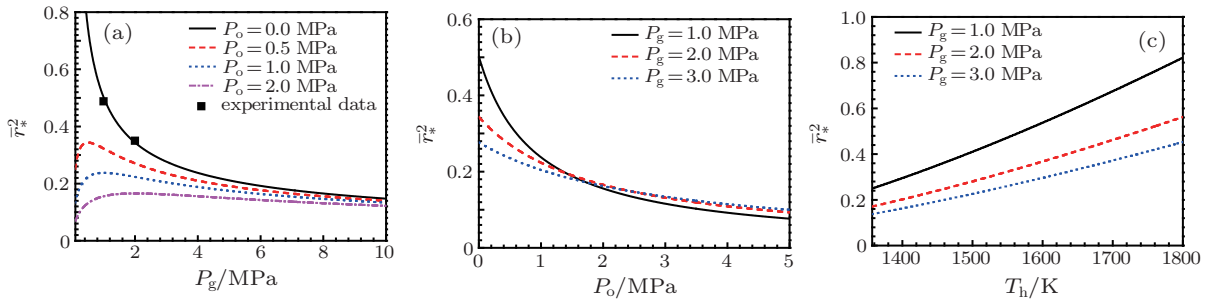


Fig. 3. (color online) Relationship of porosity with (a) P_g for the case of $T_h = 1573$ K; (b) with P_o for the case of $T_h = 1573$ K; and (c) with T_h for the case of $P_o = 0$ MPa.

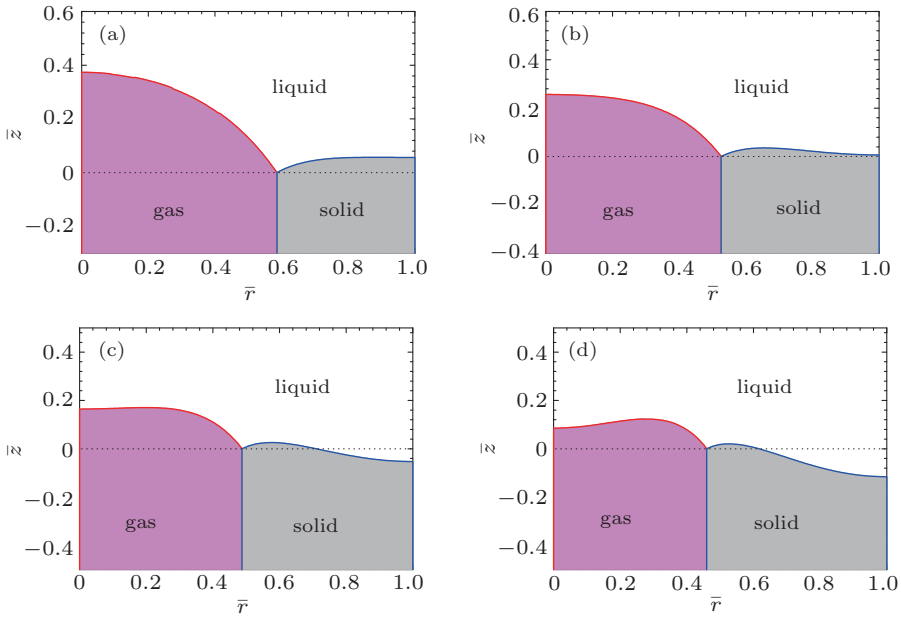


Fig. 4. (color online) Typical shapes of vertical section through symmetry axis $\bar{r} = 0$ for the case of $T_h = 1573$ K, $P_o = 0$ MPa, $V = 1 \times 10^{-4}$ m/s, $G = 1 \times 10^3$ K/m, $R = 3 \times 10^{-5}$ m, and (a) $P_g = 2$ MPa, (b) $P_g = 3$ MPa, (c) $P_g = 4$ MPa, (d) $P_g = 5$ MPa, respectively.

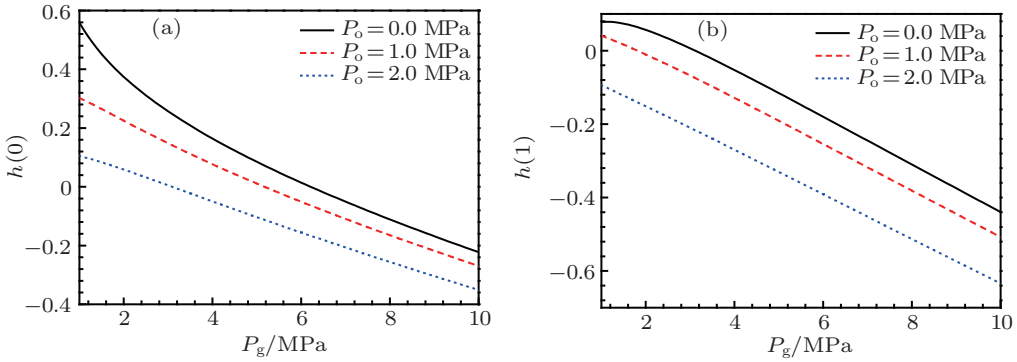


Fig. 5. (color online) Relationship of (a) $\bar{h}(0)$ and (b) $\bar{h}(1)$ with P_g for the case of $T_h = 1573$ K, $V = 1 \times 10^{-4}$ m/s, $G = 1 \times 10^3$ K/m, and $R = 3 \times 10^{-5}$ m.

4. Conclusions

Considering the nonzero surface tension, we develop a general mathematical formulation for gasar eutectic growth in directional solidification. As the Peclet number ε is a small parameter, we obtain the asymptotic steady solution using multiple scale expansion and a matching method. Effects of external pressure and temperature of the hot zone on the porosity of gasar eutectic growth under unidirectional solidification are predicted. Morphologies of both gas–liquid and gas–solid interfaces are presented for given control conditions. The results obtained also show that the steady system allows a family of solutions with a free parameter, inter-pore spacing R. In order to determine R, we are going to study the stability of gasar eutectic growth, considering unsteady gasar eutectic growth.

References

[1] Shapovalov V I 1993 (US Patent) 5181549

[2] Yamamura S, Shiota H, Murakami K and Nakajima H 2001 *Mater. Sci. Eng. A* **318** 137

[3] Park J S, Hyun S K, Suzuki S and Nakajima H 2007 *Acta Mater.* **55** 5646

[4] Nakajima H 2007 *Prog. Mater. Sci.* **52** 1091

[5] Zheng Y 1995 *Modelling of Solidification of Porous Metal-Hydrogen Alloys* (Ph.D. Thesis) (Massachusetts: Massachusetts Institute of Technology)

[6] Liu Y and Li Y 2003 *Scri. Mater.* **49** 379

[7] Drenchev L, Sobczak J, Sobczak N, Sha W and Malinov S 2007 *Acta Mater.* **55** 6459

[8] Jackson K A and Hunt J D 1966 *Trans. Metall. Soc. AIME* **236** 1129

[9] Chen Y Q, Tang X X and Xu J J 2009 *Chin. Phys. B.* **18** 671

[10] Chen Y Q, Tang X X and Xu J J 2009 *Chin. Phys. B* **18** 686

[11] Ding G L, Lin X, Huang W D and Zhou Y H 1997 *Acta Phys. Sin.* **46** 1243 (in Chinese)

[12] Huang W D, Shang B L and Zhou Y H 1991 *Acta Phys. Sin.* **40** 323 (in Chinese)

[13] Chen M W, Lan M, Wang Y Y, Wang Z D, Xu J J and Yuan L 2009 *Chin. Phys. B* **18** 1691

[14] Chen Y J and Davis S H 2001 *Acta Mater.* **49** 1363

[15] Li X M, Wang Z D and Wang Q Y 2009 *J. Appl. Phys.* **106** 053511

[16] Li X M and Wang Z D 2010 *Chin. Phys. B* **19** 126401

[17] Li X M and Wang Z D 2011 *J. Cryst. Growth* **318** 55

[18] Li X M 2011 *Research of the Dendritic Pattern of a Binary Alloy under Effect of the Forced Flow and the Mushy Zone of Dendritic Growth* (Ph.D. Thesis) (Beijing: University of Science and Technology of Beijing) (in Chinese)